NACA RM L50A12

NACA

RESEARCH MEMORANDUM

AERODYNAMIC CHARACTERISTICS OF A WING WITH QUARTER-CHORD LINE SWEPT BACK 60°, ASPECT RATIO 2, TAPER RATIO 0.6, AND NACA 65A006 AIRFOIL SECTION

TRANSONIC-BUMP METHOD

By Boyd C. Myers, II and Thomas J. King, Jr.

Langley Aeronautical Laboratory
Langley Air Force Base, Va.

NATIONAL ADVISORY COMMITTEE
FOR AERONAUTICS

WASHINGTON

February 24, 1950
Declassified August 23, 1954

NACA RM L50A12

NATIONAL ADVISORY COMMITTEE FOR AERONAUTICS

RESEARCH MEMORANDUM

AERODYNAMIC CHARACTERISTICS OF A WING WITH QUARTER-CHORD LINE SWEPT BACK 60°, ASPECT RATIO 2, TAPER RATIO 0.6, AND NACA 65A006 AIRFOIL SECTION

TRANSONIC-BUMP METHOD

By Boyd C. Myers, II and Thomas J. King, Jr.

SUMMARY

As part of a transonic research program, a series of wing-body combinations is being investigated in the Langley high-speed 7- by 10-foot tunnel over a Mach number range of about 0.60 to 1.20, utilizing the transonic-bump test technique.

This paper presents the results of the investigation of a wing-alone and a wing-fuselage configuration employing a wing with quarter-chord line swept back 60°, aspect ratio 2, taper ratio 0.6, and an NACA 65A006 airfoil section. The results are presented as lift, drag, pitching-moment, and bending-moment coefficients for both configurations. In addition, effective downwash angles and point dynamic pressures for a range of tail heights at a probable tail length are presented for the two configurations investigated. Only a brief analysis was made in order to facilitate the publishing of the data.

INTRODUCTION

A series of wing-fuselage combinations is being investigated in the Langley high-speed 7- by 10-foot tunnel to study the effects of wing geometry on longitudinal stability characteristics at transonic speeds. In the research program utilizing the transonic-bump technique, a Mach number range of about 0.60 to 1.20 is investigated.

This paper presents the results of the investigation of the wing-alone and wing-fuselage configurations employing a wing with the

quarter-chord line swept back 60°, aspect ratio 2, taper ratio 0.6, and an NACA 65A006 airfoil section parallel to the free stream. The results of a 60° sweptback wing of aspect ratio 4, which was part of the present transonic program, are presented in reference 1.

MODEL AND APPARATUS

The wing of the semispan model had 60° of sweepback referred to the quarter-chord line, aspect ratio 2, taper ratio 0.6, and an NACA 65A006 airfoil section (reference 2) parallel to the free stream. The wing was made of beryllium copper and the fuselage of brass. A two-view drawing of the model is presented in figure 1 and ordinates of the fuselage of actual fineness ratio 10 (achieved by cutting off the rear portion of a streamline body of fineness ratio 12) are given in table I.

The model was mounted on an electrical strain-gage balance enclosed in the bump and the lift, drag, pitching moment, and bending moment about the model plane of symmetry were measured with calibrated potentiometers.

Effective downwash angles were determined for a range of tail heights by measuring the floating angles of five free-floating tails with calibrated slide-wire potentiometers. Details of the floating tails are given in figures 2 and 3, while a view of the model mounted on the bump showing three of the floating tails is given in figure 4. The tails used in this investigation are the same as those used in reference 1.

A total-pressure rake was used to determine the dynamic-pressure ratios for a range of tail heights along a line which contained the 25-percent mean-aerodynamic-chord point of the free-floating tails. The total-pressure tubes were spaced 1/8 inch apart near the chord line extended and 1/4 inch apart elsewhere.

COEFFICIENTS AND SYMBOLS

C_L lift coefficient $\left(\frac{\text{Twice semispan lift}}{qS}\right)$

C_D drag coefficient $\left(\frac{\text{Twice semispan drag}}{qS}\right)$

C_m pitching-moment coefficient referred to $0.25\bar{c}$ $\left(\frac{\text{Twice semispan pitching moment}}{qS\bar{c}}\right)$

C_B bending-moment coefficient about root chord line (at plane of symmetry) $\left(\frac{\text{Root bending moment}}{q \frac{S}{2} \frac{b}{2}}\right)$

q effective dynamic pressure over span of model, pounds per square foot $\left(\rho V^2/2\right)$

S twice wing area of semispan model, 0.125 square foot

$\bar{c}$ mean aerodynamic chord of wing, 0.255 foot; based on relationship $\frac{2}{S}\int_0^{b/2} c^2 dy$ (using the theoretical tip)

c local wing chord, parallel to plane of symmetry

$\bar{c}_t$ mean aerodynamic chord of tail

b twice span of semispan model, 0.50 foot

y spanwise distance from plane of symmetry

y_{cp} lateral center of pressure

ρ air density, slugs per cubic foot

V free-stream velocity, feet per second

M effective Mach number over span of model

M_l local Mach number

M_a average local Mach number, chordwise

R Reynolds number of wing based on $\bar{c}$

α angle of attack, degrees

ϵ effective downwash angle, degrees

$\frac{q_{wake}}{q}$ ratio of point dynamic pressure, along a line containing the quarter-chord points of the mean aerodynamic chords of the free-floating tails, to the local free-stream dynamic pressure

h_t tail height relative to wing chord plane extended, percent semispan; positive for tail positions above chord plane extended

Subscripts:

M at constant Mach number

$C_L = 0$ at zero lift

TESTS AND CORRECTIONS

The tests were conducted in the Langley high-speed 7- by 10-foot tunnel by use of an adaptation of the NACA wing-flow technique for obtaining transonic speeds. The method used involved the mounting of a model in the high-velocity flow field generated over the curved surface of a bump located on the tunnel floor. (See reference 3.)

Typical contours of local Mach numbers in the region of the model location on the bump, obtained from surveys with no model in position, are shown in figure 5. There is a Mach number gradient which resulted in a difference of about 0.03 over the span of the model at the lowest and highest Mach numbers with a maximum difference of about 0.05 present at a Mach number of about 1.0. The chordwise Mach number difference varied from about 0.01 to 0.02. No attempt has been made to evaluate the effects of these spanwise and chordwise variations in Mach number. The long-dash lines shown near the wing root represent a local Mach number 5 percent below the maximum value and indicate the extent of the bump boundary layer. The effective test Mach number was obtained from contour charts similar to those presented in figure 5 from the relationship

$$M = \frac{2}{S}\int_0^{b/2} cM_a \, dy$$

The variation of mean test Reynolds number with Mach number is shown in figure 6. The boundaries in the figure indicate the range in Reynolds number caused by variations in test conditions during the course of the investigation.

Force and moment data, effective downwash angles, and the ratio of dynamic pressure at 25 percent of the mean aerodynamic chords of the free-floating tails to free-stream dynamic pressure were obtained for the model configurations tested through a Mach number range of 0.70 to 1.18 and an angle-of-attack range of -2° to 10°.

The end-plate tares on drag were obtained through the test Mach number range at zero angle of attack by testing the model configurations without end plates. For these tests a gap of about 1/16 inch was maintained between the wing root and the bump surface, and a sponge-wiper seal was fastened to the wing butt beneath the surface of the bump to prevent leakage. (See fig. 7.) The drag end-plate tares were assumed to be invariant with angle of attack and the tares obtained at zero angle of attack were applied to all drag data. Jet-boundary corrections have not been evaluated inasmuch as the boundary conditions to be satisfied are not rigorously defined. However, inasmuch as the effective-flow field is large compared with the span and chord of the model, these corrections are believed to be small. Considerations of the results of static loading of the wing of reference 1 indicate that the deflection of the present wing under load would be negligible.

From measurements of tail floating angles without a model installed, it was determined that a tail spacing of 2 inches relative to the wing chord plane would produce negligible interference effects of reflected shock waves on the tail floating angles. Downwash angles for the wing-alone configuration were therefore obtained simultaneously for the middle, highest, and lowest tail positions in one series of tests and for the two intermediate positions in succeeding runs. (See fig. 3.) For the wing-fuselage tests, the effective downwash angles at the chord plane extended were determined by mounting a free-floating tail on the center line and at the surface of the fuselage; thus this tail was placed at a slightly different spanwise position than the other tails. The downwash angles presented are increments from the tail floating angles without a model in position. It should be noted that the floating angles measured are actually a measure of the angle of zero pitching moment about the tail-pivot axis rather than the angle of zero lift. It has been estimated that, for the tail arrangement used, a 2° spanwise downwash gradient over the tail will result in an error of about 0.2° in the resultant floating angle.

Total-pressure readings were obtained at constant angles of attack through the Mach number range without an end plate on the model to eliminate end-plate wakes and with the gap around the model sealed to minimize any leakage effects. The pressures have been corrected for bow-wave loss and the static-pressure values used in computing dynamic-pressure ratios were obtained without a model in position.

RESULTS AND DISCUSSION

A table of the figures presenting the results follows:

Unless otherwise noted, the discussion is based on the summary curves presented in figure 14. The slopes have been averaged at $C_L = 0$ over a lift-coefficient range of ± 0.1.

Lift and Drag Characteristics

The lift-curve slope at zero lift of the wing-alone configuration had very little variation throughout the Mach number range but increased from a value of 0.040 at $M = 0.70$ to a maximum value of about 0.046 near $M = 1.03$. This value of 0.040 at $M = 0.70$ compared with a theoretical value of about 0.036 estimated for this Mach number by the method of reference 4. The addition of the fuselage increased the lift-curve slope about 8 percent throughout the test Mach number range. The nonlinearity of the lift curves (figs. 8 and 9) is congruous with the effect of aspect ratio and sweepback encountered on similar plan forms at low speeds and at higher Reynolds numbers (reference 5).

The drag rise at zero lift occurred at a Mach number of about 1.03 for both the wing-alone and wing-fuselage configurations. The zero lift drag value at $M = 0.70$ of 0.004 remained constant up to $M = 1.00$ and increased gradually thereafter to a value of 0.010 at the highest test Mach number. The addition of the fuselage increased the total drag coefficient by an increment of about 0.007 throughout the subsonic Mach number range. This increment increased to a value of of 0.018 at $M = 1.18$. The variation of drag coefficient with Mach number for both configurations is notably similar to that of the wing of reference 1 although the absolute values are somewhat lower for the present wing.

The lateral center of pressure for the wing alone ($C_L = \pm 0.1$) was located at 43 percent of the semispan at a Mach number of 0.70. This value compares with a theoretical value of 44.5 percent semispan

estimated by use of reference 4. It should be noted that for the wing-alone configuration, y_{cp} remains practically constant with Mach number except for an inboard shift of about 3 percent semispan in the Mach number range from $M = 0.95$ to $M = 1.10$. The addition of the fuselage moved the lateral center of pressure inboard about 5 percent semispan up to $M = 1.07$. Above this Mach number the effect of the fuselage was somewhat greater and resulted in about a 10-percent inboard movement of the lateral center of pressure at $M = 1.18$.

Pitching-Moment Characteristics

Near zero lift the aerodynamic-center location for the wing-alone configuration was at 25 percent of the mean aerodynamic chord $\left(\frac{\partial C_m}{\partial C_L}\right)_M = 0$ up to $M = 0.85$. This value compared with an aerodynamic-center location of about 23 percent mean aerodynamic chord estimated for $M = 0$ by the method of reference 4. The addition of the fuselage moved the aerodynamic center rearward about 4 percent mean aerodynamic chord up to $M = 1.05$. Above this Mach number the stabilizing influence of the fuselage is reduced and becomes zero at $M = 1.18$. The stabilizing influence of the fuselage on a wing of 60° sweep has been previously noted experimentally for this Mach number range (reference 1).

Unlike the results of the wing of reference 1, it is noted that for both wing and wing-fuselage configurations (figs. 8 and 9) there is no evidence of unstable pitching-moment trends at the highest lift coefficients obtained for all test Mach numbers. These pitching-moment trends are very similar to those obtained at low speeds for an almost identical plan-form configuration (reference 5).

Downwash and Dynamic-Pressure Surveys in Region of the Tail Plane

The downwash gradient $\partial\epsilon/\partial\alpha$ near zero lift for the wing alone (fig. 14) had little variation with Mach number for constant tail heights of 0 percent and ±30 percent semispan.

The addition of the fuselage increased the downwash gradient $\partial\epsilon/\partial\alpha$ (fig. 12) for all tail heights up to a Mach number of 0.98 with the greatest effect occurring at zero tail-height position. It should be noted that the effective downwash angles are determined over a slightly more outboard spanwise region for the fuselage-tail configuration ($h_t = 0$) than for the wing-alone middle tail (see figs. 2 and 3). Above $M = 0.98$ the downwash gradient was about the same as the wing-alone gradients. At $M = 1.15$, however, $\partial\epsilon/\partial\alpha$ for the wing fuselage was about 25 percent less than the wing alone for all tail heights.

The results of the point-dynamic-pressure surveys made along a line perpendicular to the chord plane extended (at $\alpha = 0$) and containing the 25-percent mean-aerodynamic-chord point of the free-floating tails are presented in figure 13. There was little change in the wake characteristics for all test angles of attack for the wing-alone configuration throughout the Mach number range.

The addition of the fuselage had very little effect on the dynamic-pressure characteristics for all test angles of attack up to $M = 1.00$. Above this Mach number the addition of the fuselage increased the loss in dynamic pressure at the tail, especially at $\alpha = 10^\circ$, for all tail heights other than the tail position at the wake center line.

It should be noted that for both the wing-alone and wing-fuselage configurations at all Mach numbers the wake center line moved from the zero tail-height position at $\alpha = 0^\circ$ to about 8-percent-semispan tail-height position above the wing chord plane at $\alpha = 10^\circ$.

Langley Aeronautical Laboratory
National Advisory Committee for Aeronautics
Langley Air Force Base, Va.

REFERENCES

1. King, Thomas J., Jr., and Myers, Boyd C., II: Aerodynamic Characteristics of a Wing with Quarter-Chord Line Swept Back 60°, Aspect Ratio 4, Taper Ratio 0.6, and NACA 65A006 Airfoil Section. Transonic-Bump Method. NACA RM L9G27, 1949.

2. Lortin, Laurence K., Jr.: Theoretical and Experimental Data for a Number of NACA 6A-Series Airfoil Sections. NACA Rep. 903, 1948.

3. Schneiter, Leslie E. and Ziff, Howard L.: Preliminary Investigation of Spoiler Lateral Control on a 42° Sweptback Wing at Transonic Speeds. NACA RM L7F19, 1947.

4. DeYoung, John: Theoretical Additional Span Loading Characteristics of Wing with Arbitrary Sweep, Aspect Ratio, and Taper Ratio. NACA TN 1491, 1947.

5. Lowry, John G., and Schneiter, Leslie E.: Investigation at Low Speed of the Longitudinal Stability Characteristics of a 60° Swept-Back Tapered Low-Drag Wing. NACA TN 1284, 1947.

TABLE I.- FUSELAGE ORDINATES

[Basic fineness ratio 12; actual fineness ratio 10 achieved by cutting off the rear one-sixth of the body; $\bar{c}/4$ located at $l/2$]

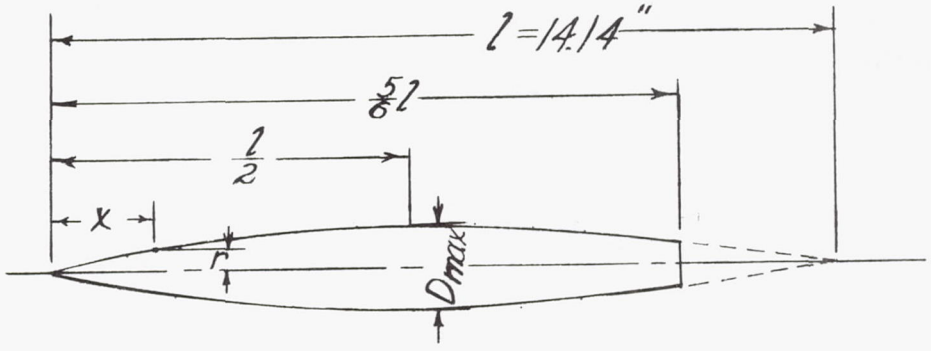

Ordinates			
x/l	r/l	x/l	r/l
0	0	0	0
.005	.00231	.4500	.04143
.0075	.00298	.5000	.04167
.0125	.00428	.5500	.04130
.0250	.00722	.6000	.04024
.0500	.01205	.6500	.03842
.0750	.01613	.7000	.03562
.1000	.01971	.7500	.03128
.1500	.02593	.8000	.02526
.2000	.03090	.8338	.02000
.2500	.03465	.8500	.01852
.3000	.03741	.9000	.01125
.3500	.03933	.9500	.00439
.4000	.04063	1.0000	0
L. E. radius = 0.0005l			

NACA

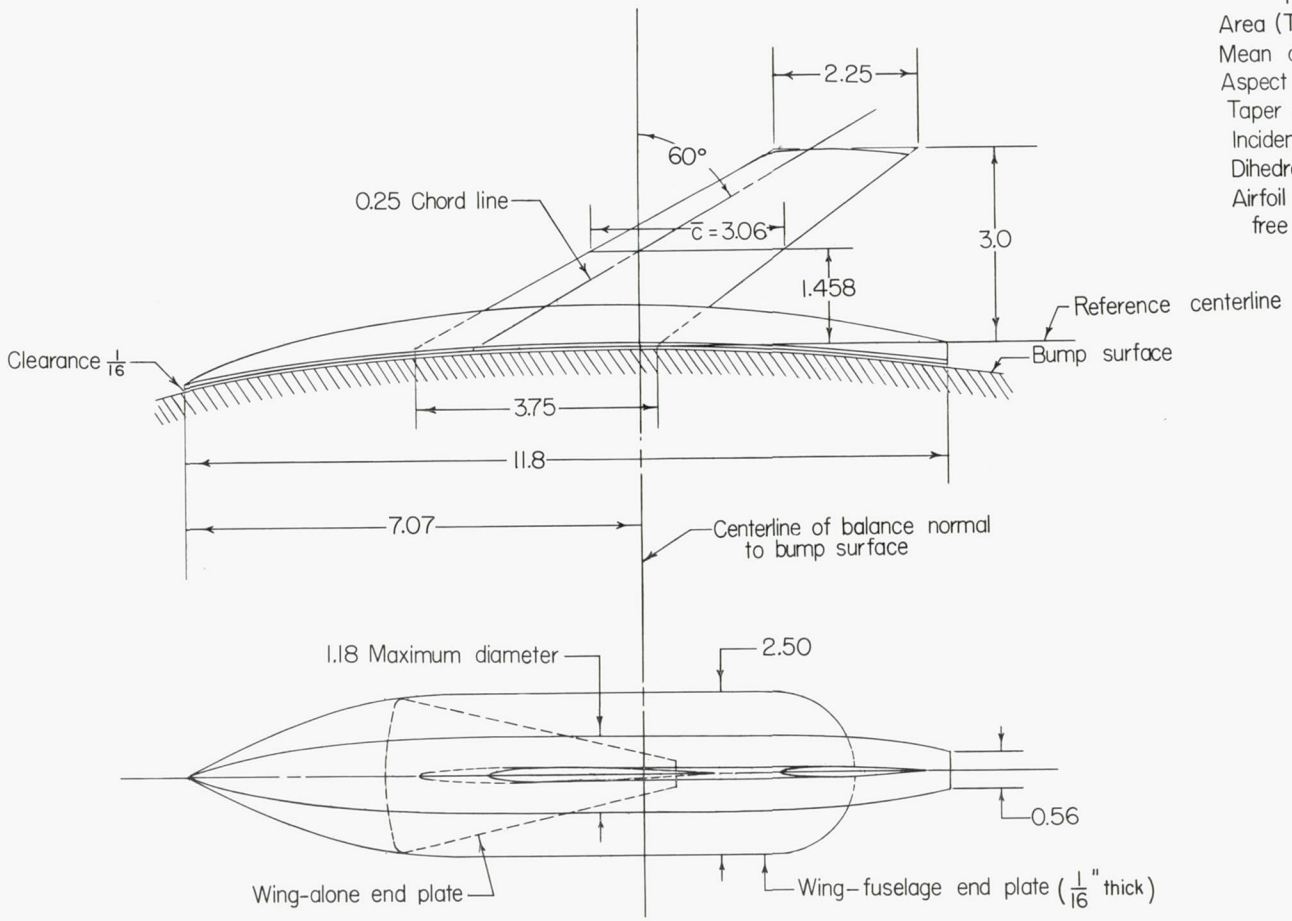

Tabulated Wing Data

Area (Twice semispan)	0.125 sq ft
Mean aerodynamic chord	0.255 ft
Aspect ratio	2.0
Taper ratio	0.6
Incidence	0.0°
Dihedral	0.0°
Airfoil section parallel to free stream	NACA 65A006

Figure 1.- General arrangement of model with 60° sweptback wing, aspect ratio 2, taper ratio 0.6, and NACA 65A006 airfoil. All dimensions are in inches.

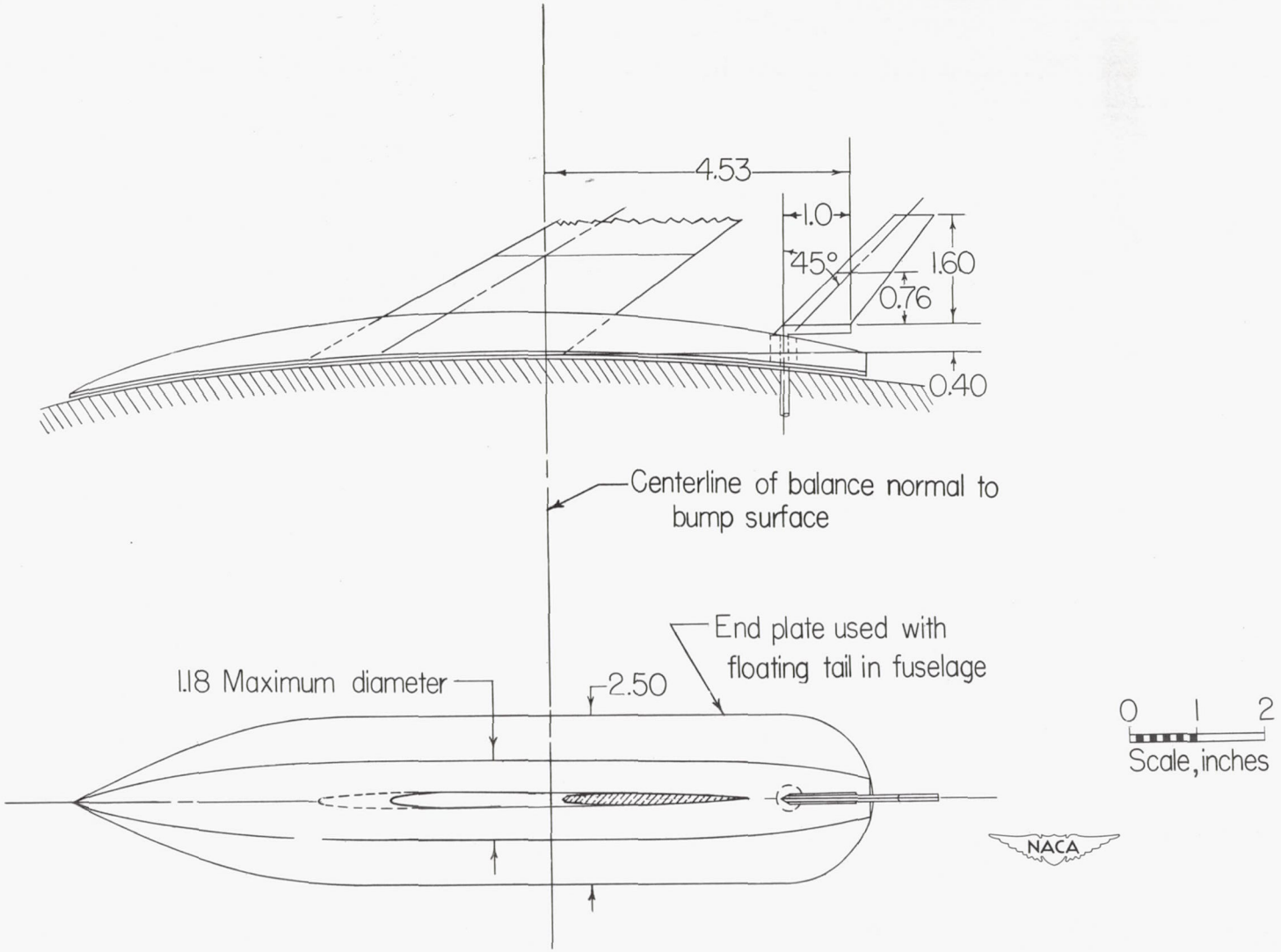

Figure 2.- Details of wing fence and free-floating tail mounted on a model with 60° sweptback wing, aspect ratio 2, taper ratio 0.6, and NACA 65A006 airfoil. All dimensions are in inches.

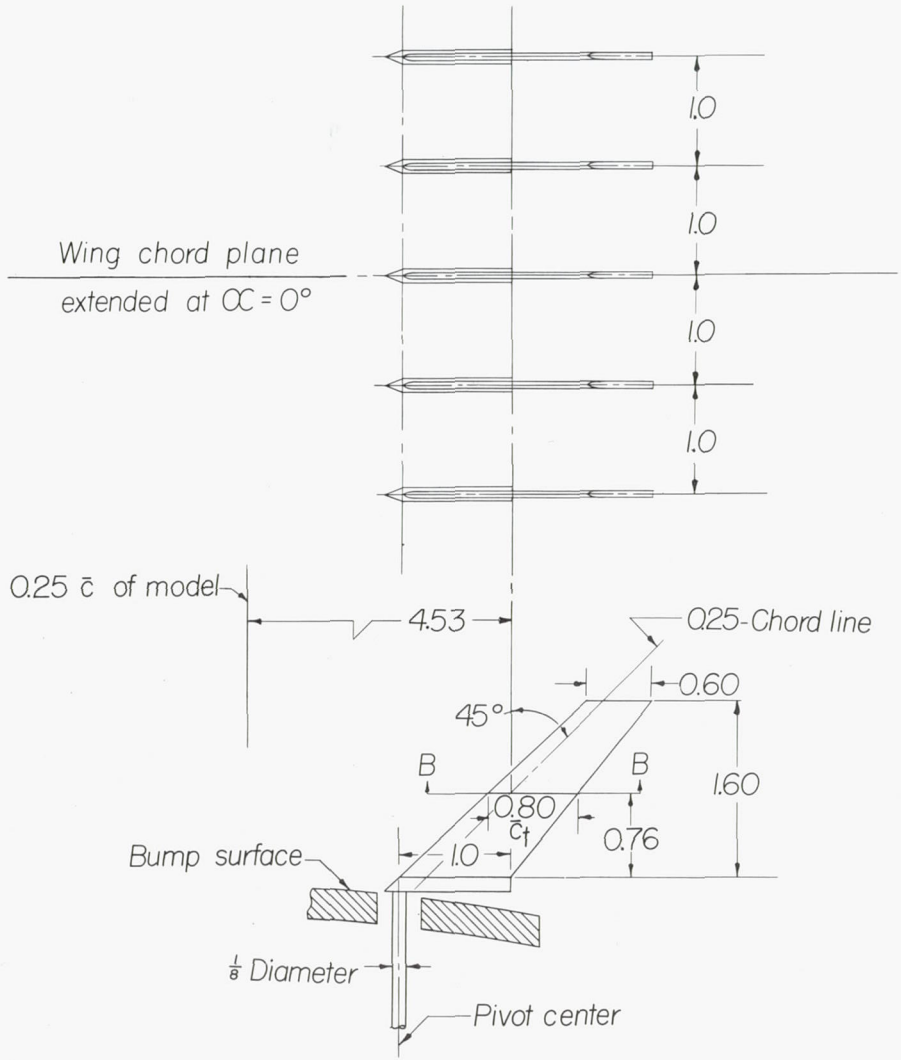

Floating-tail geometry

Area (Twice semispan)	0.0178 sq ft
Aspect ratio	4.0
Taper ratio	0.60

Section B-B

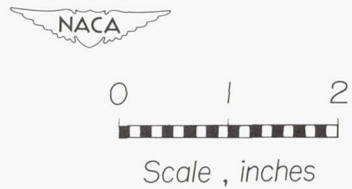

Figure 3.- Details of free-floating tails used in surveys behind model with 60° sweptback wing, aspect ratio 2, taper ratio 0.6, and NACA 65A006 airfoil. All dimensions are in inches.

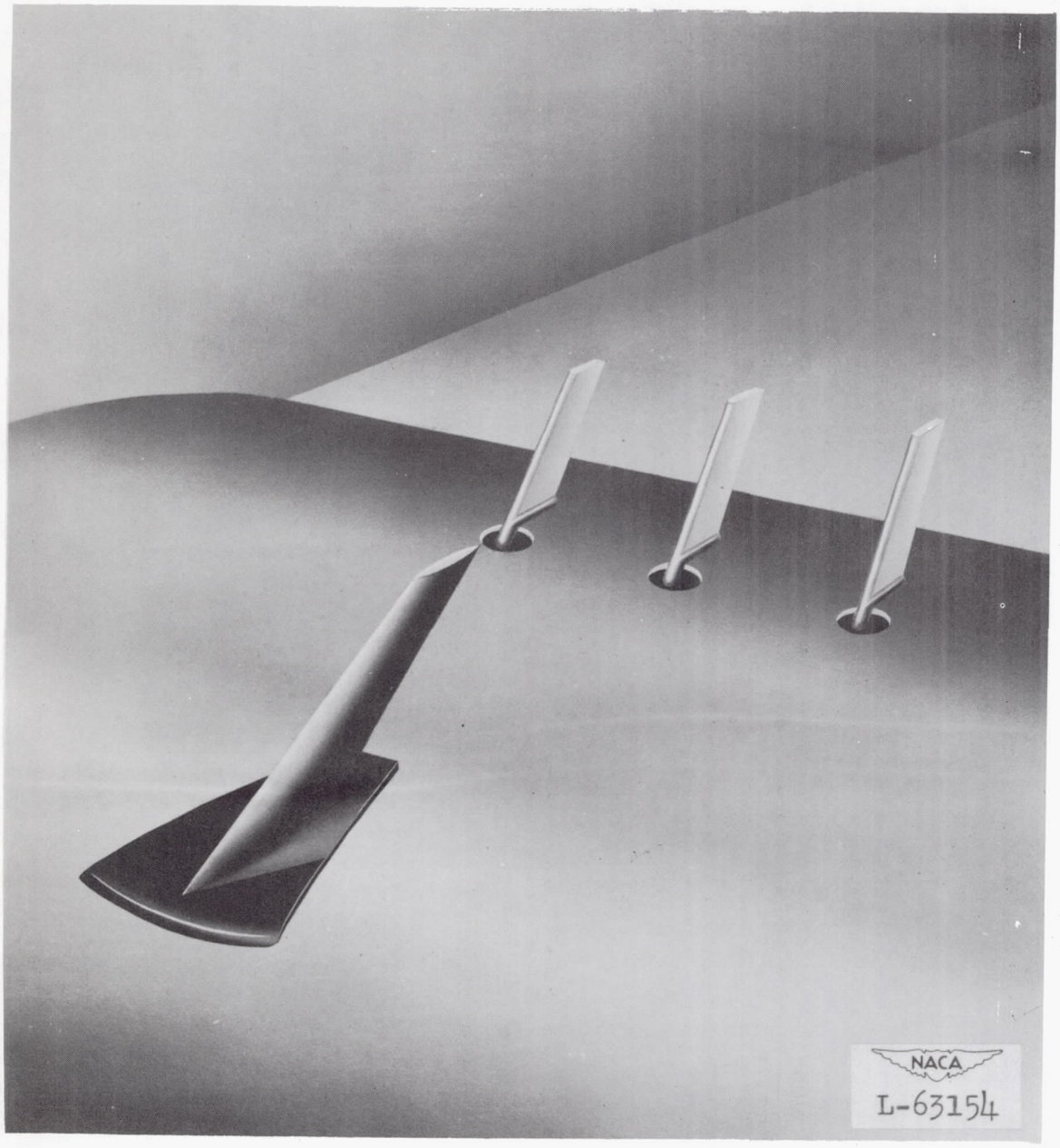

Figure 4.- A pictorial view of the model wing with quarter-chord line swept back 60°, aspect ratio 2, taper ratio 0.6, and NACA 65A006 airfoil section showing free-floating tails.

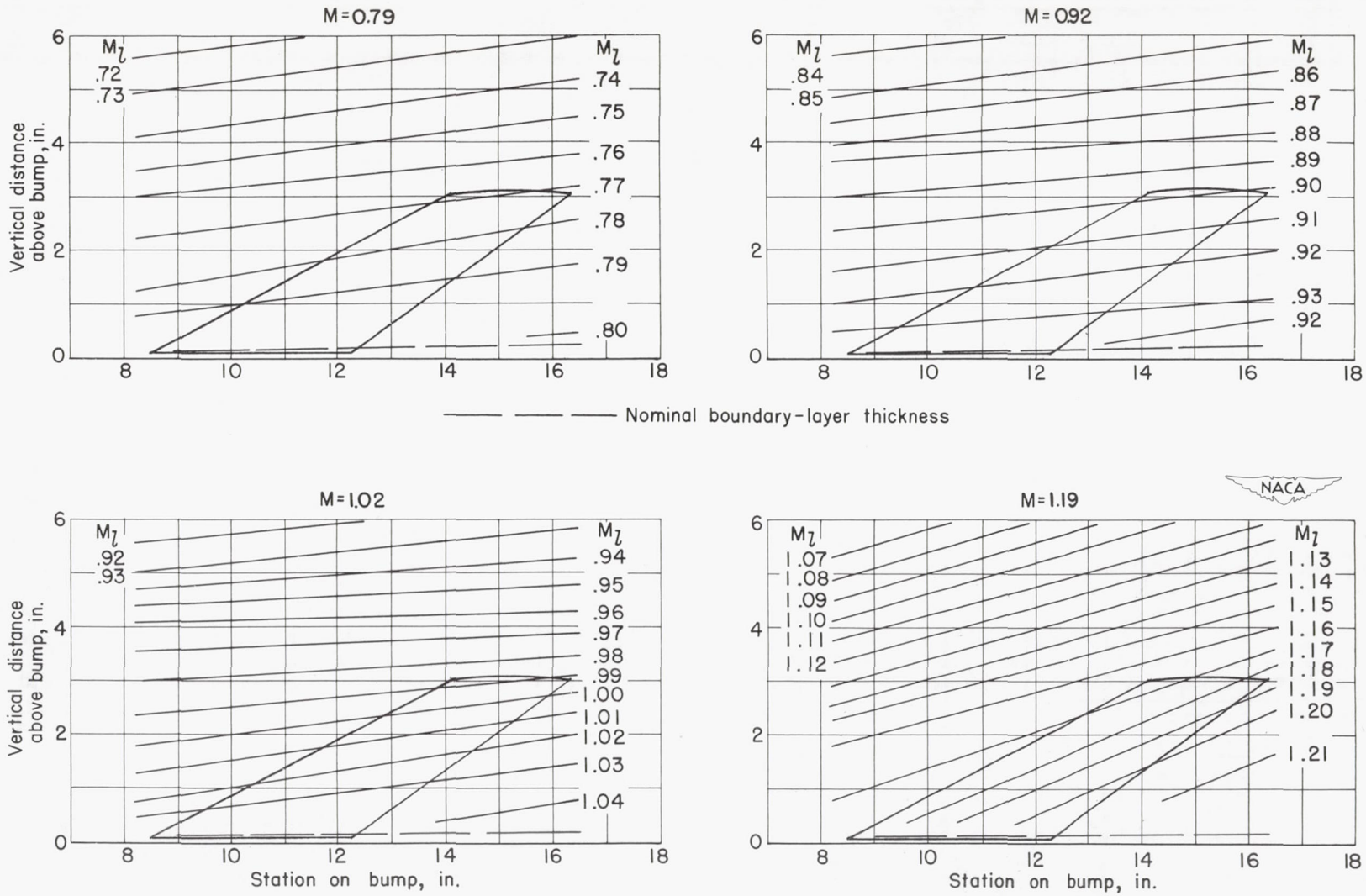

Figure 5.- Typical Mach number contours over transonic bump in region of model location.

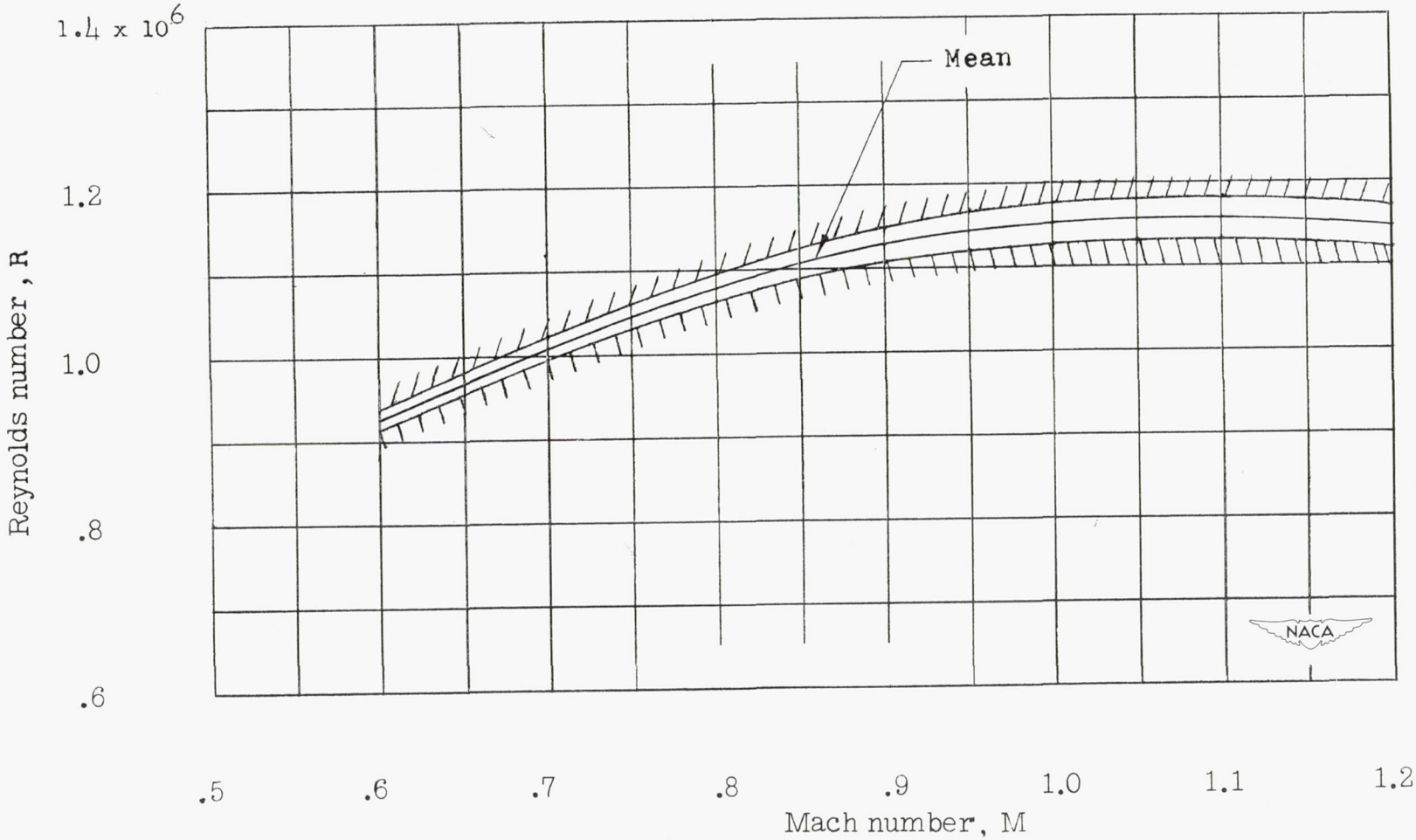

Figure 6.- Variation of test Reynolds number with Mach number for a model with 60° sweptback wing, aspect ratio 2, taper ratio 0.6, and NACA 65A006 airfoil.

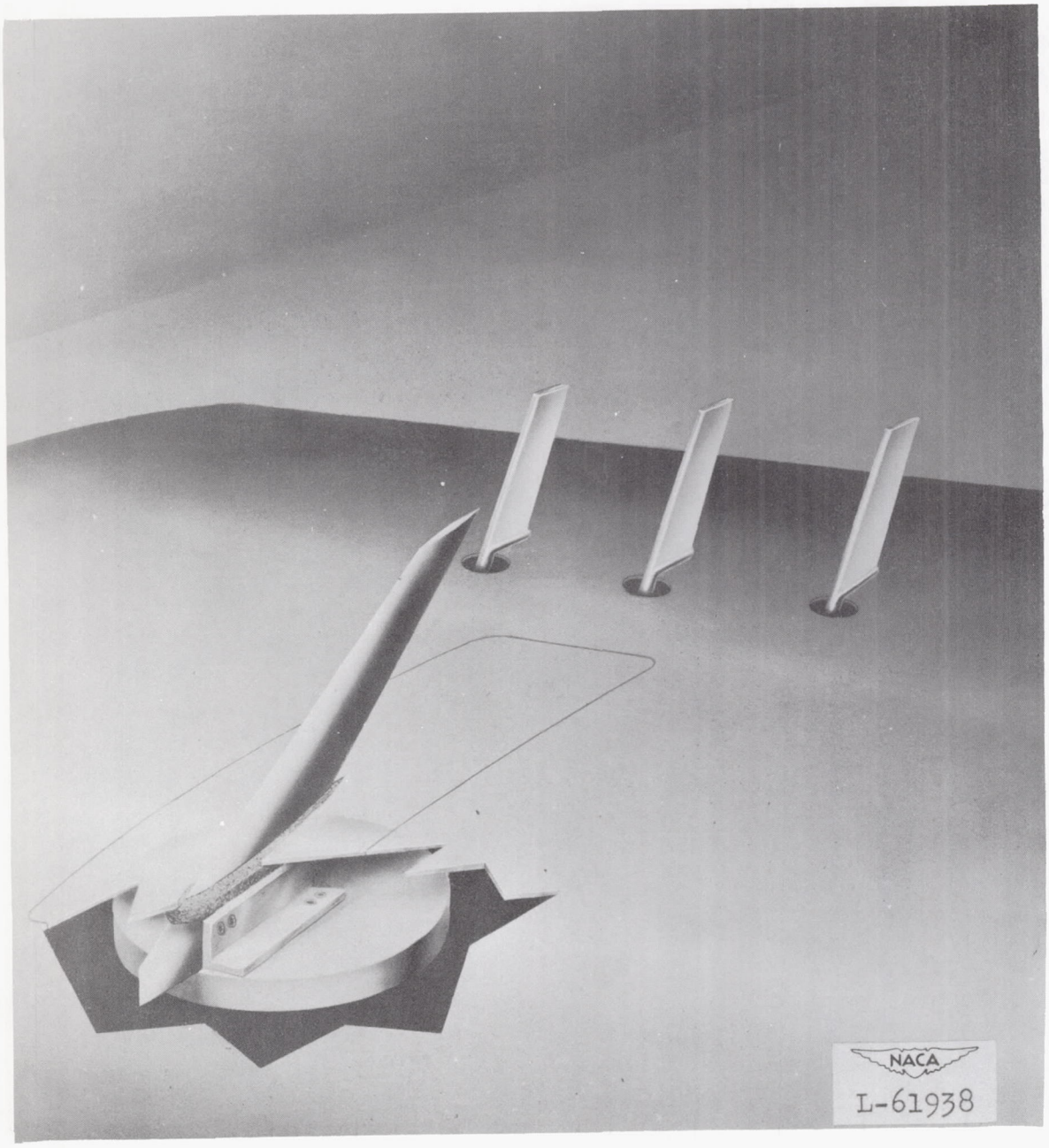

Figure 7.- A pictorial view showing sponge-wiper-seal installation on the model wing with quarter-chord line swept back 60°, aspect ratio 2, taper ratio 0.6, and NACA 65A006 airfoil section.

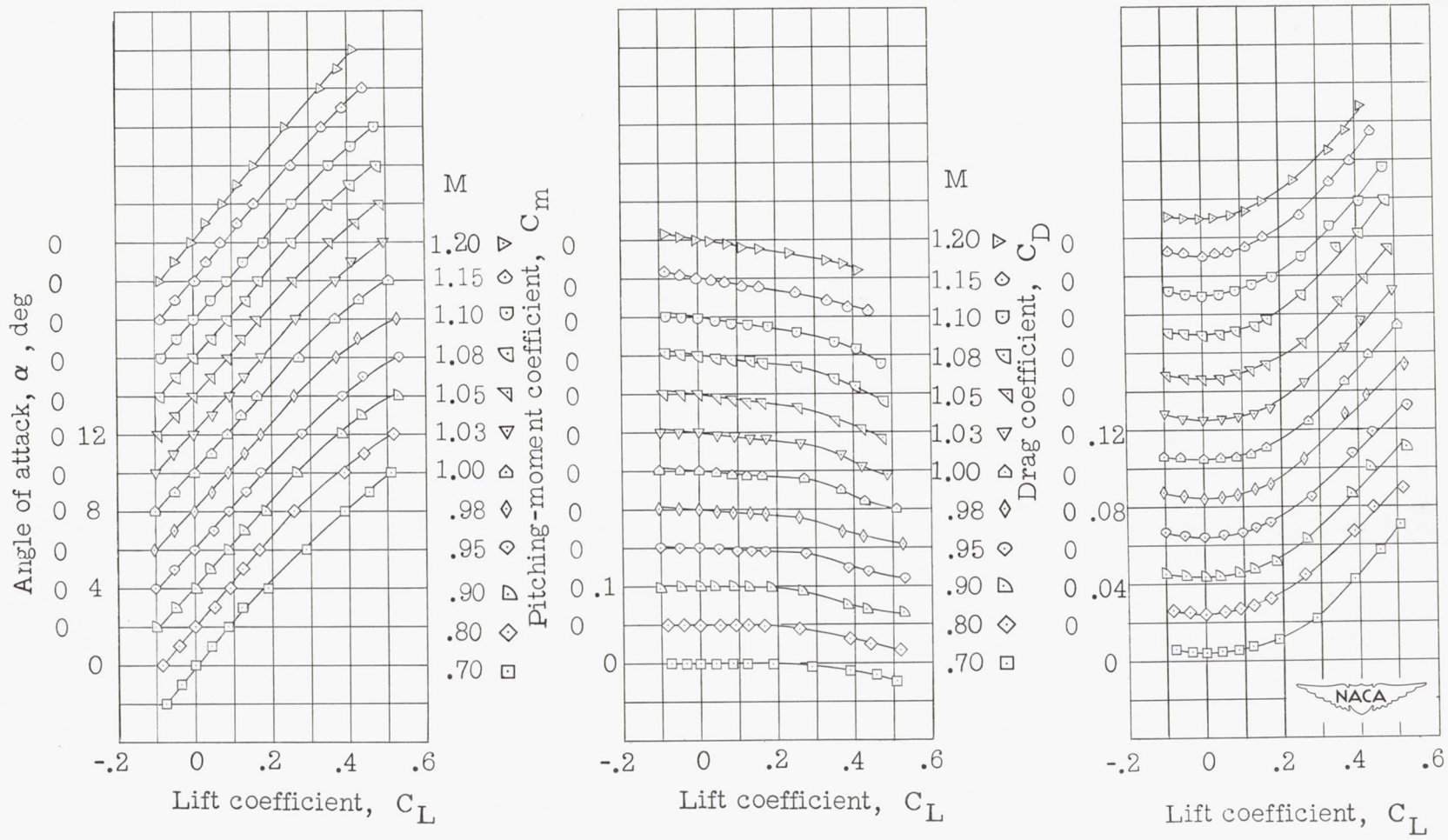

Figure 8.- Wing-alone aerodynamic characteristics for a model with 60° sweptback wing, aspect ratio 2, taper ratio 0.6, and NACA 65A006 airfoil.

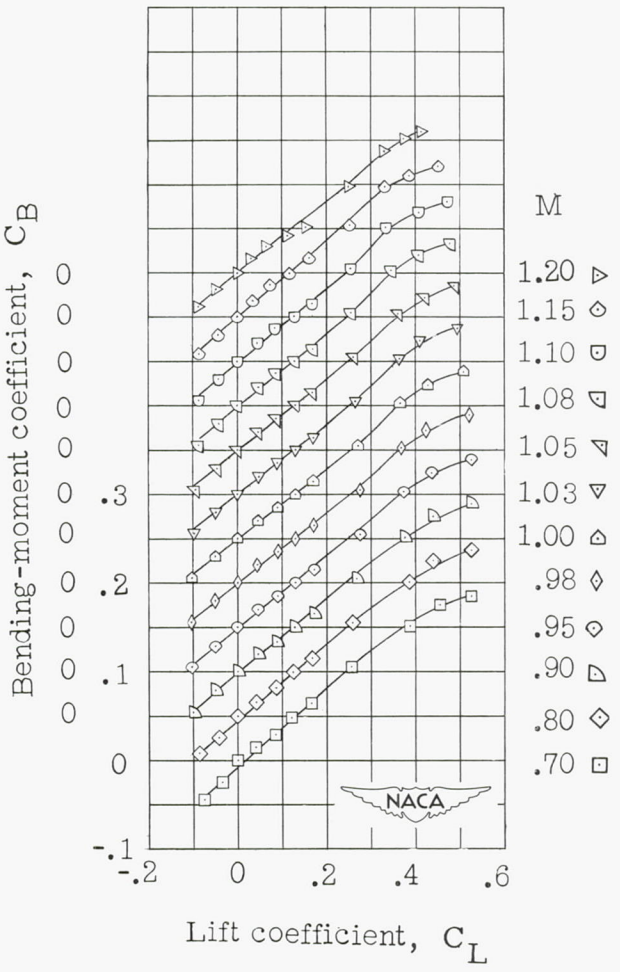

Figure 8.- Concluded.

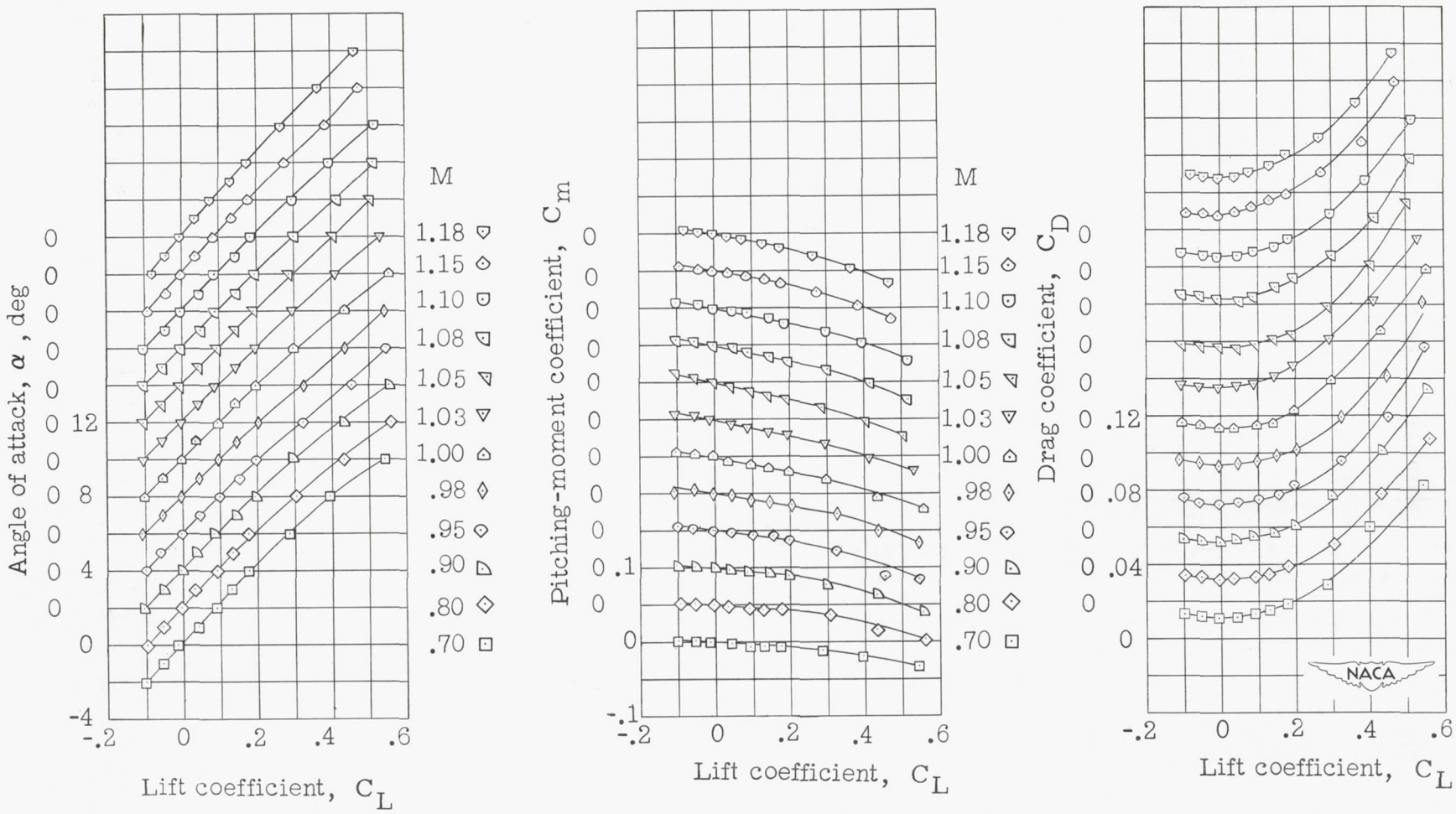

Figure 9.- Wing-fuselage aerodynamic characteristics for a model with 60° sweptback wing, aspect ratio 2, taper ratio 0.6, and NACA 65A006 airfoil.

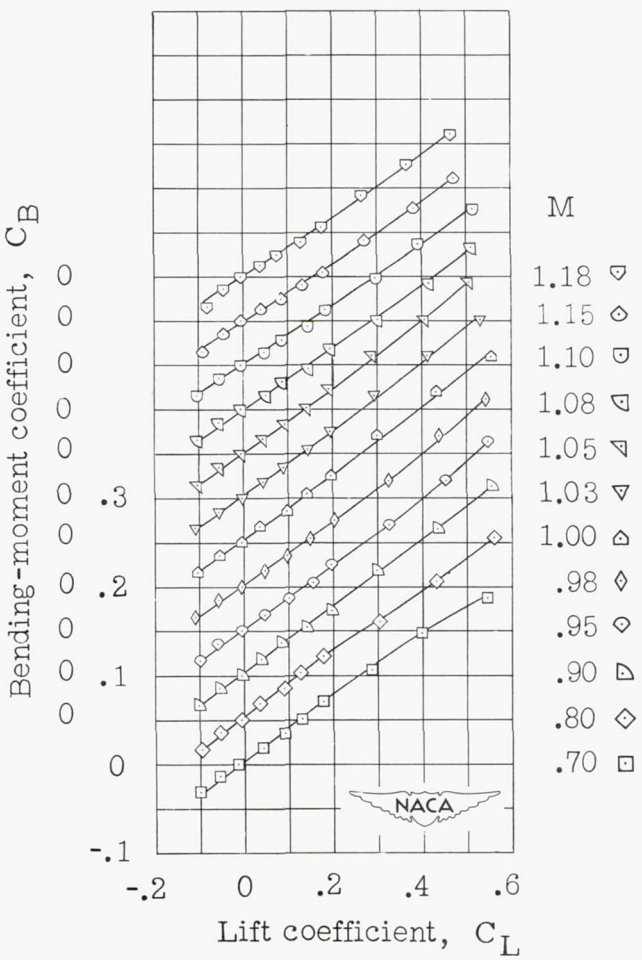

Figure 9.- Concluded.

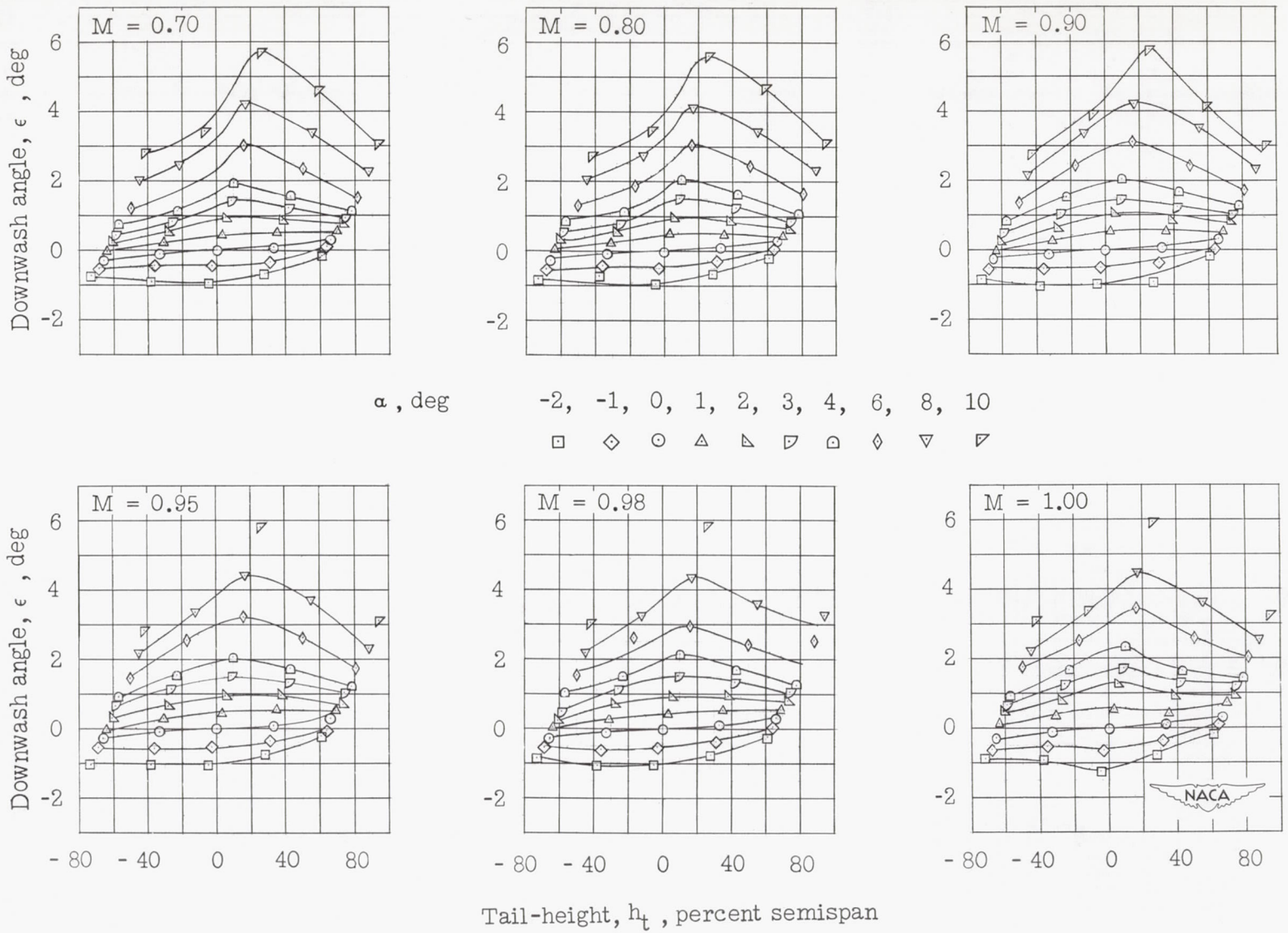

Figure 10.- Effective downwash angles in region of tail plane for a model with 60° sweptback wing, aspect ratio 2, taper ratio 0.6, and NACA 65A006 airfoil. Wing alone.

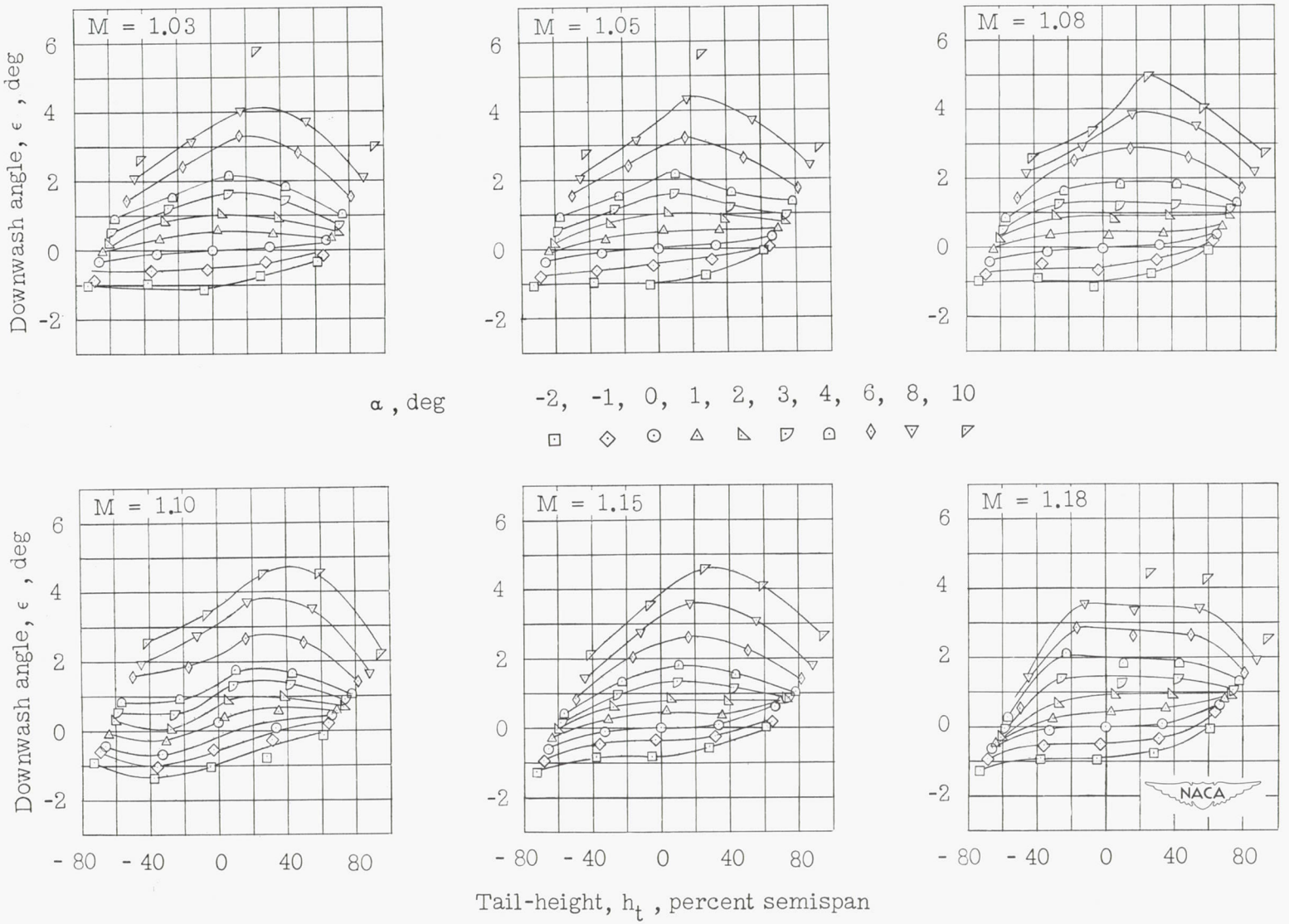

Figure 10.- Concluded.

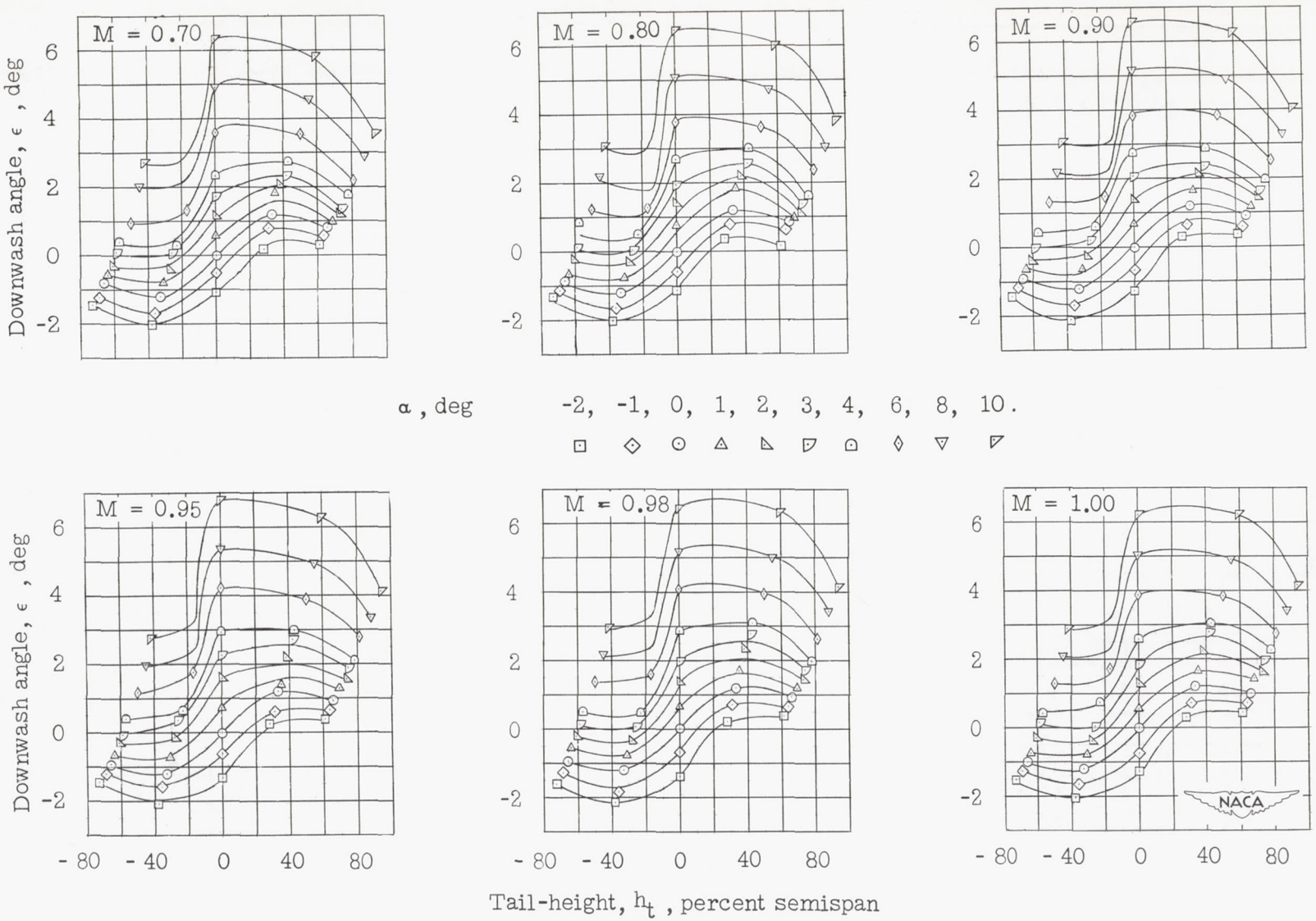

Figure 11.- Effective downwash angles in region of tail plane for a model with 60° sweptback wing, aspect ratio 2, taper ratio 0.6, and NACA 65A006 airfoil. Wing-fuselage.

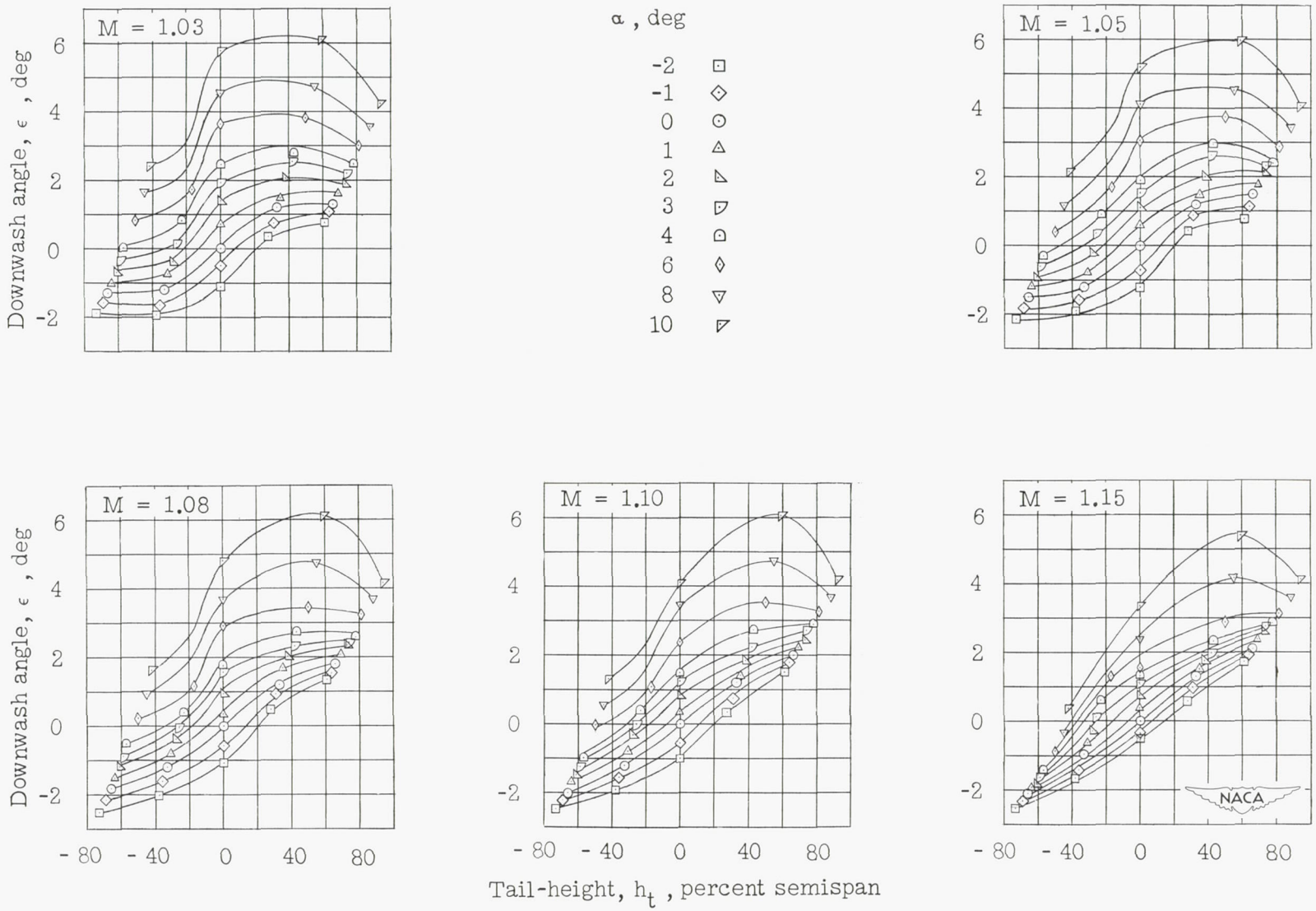

Figure 11.- Concluded.

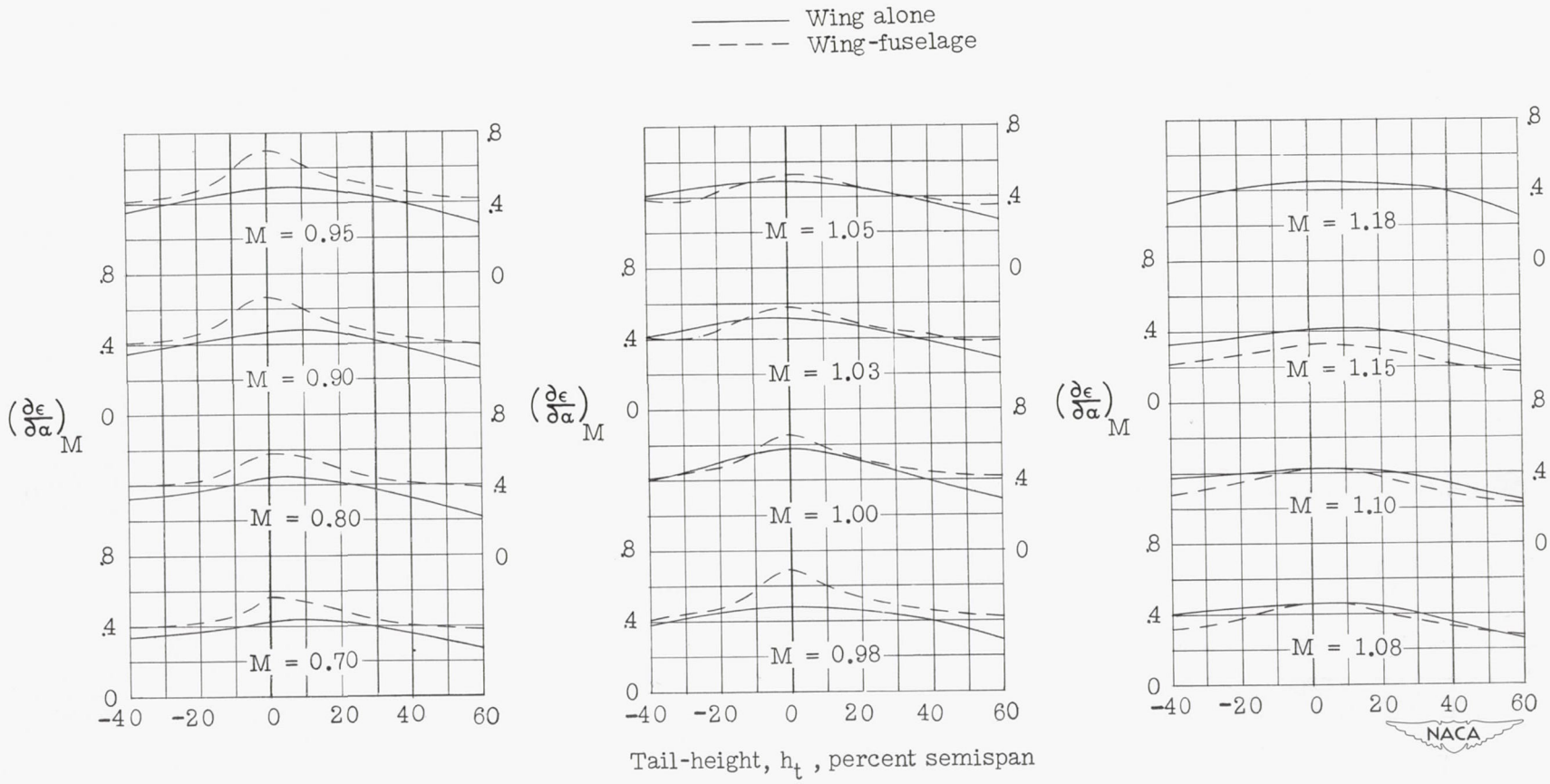

Figure 12.- Variation with tail height of downwash gradient for a model with 60° sweptback wing, aspect ratio 2, taper ratio 0.6, and NACA 65A006 airfoil.

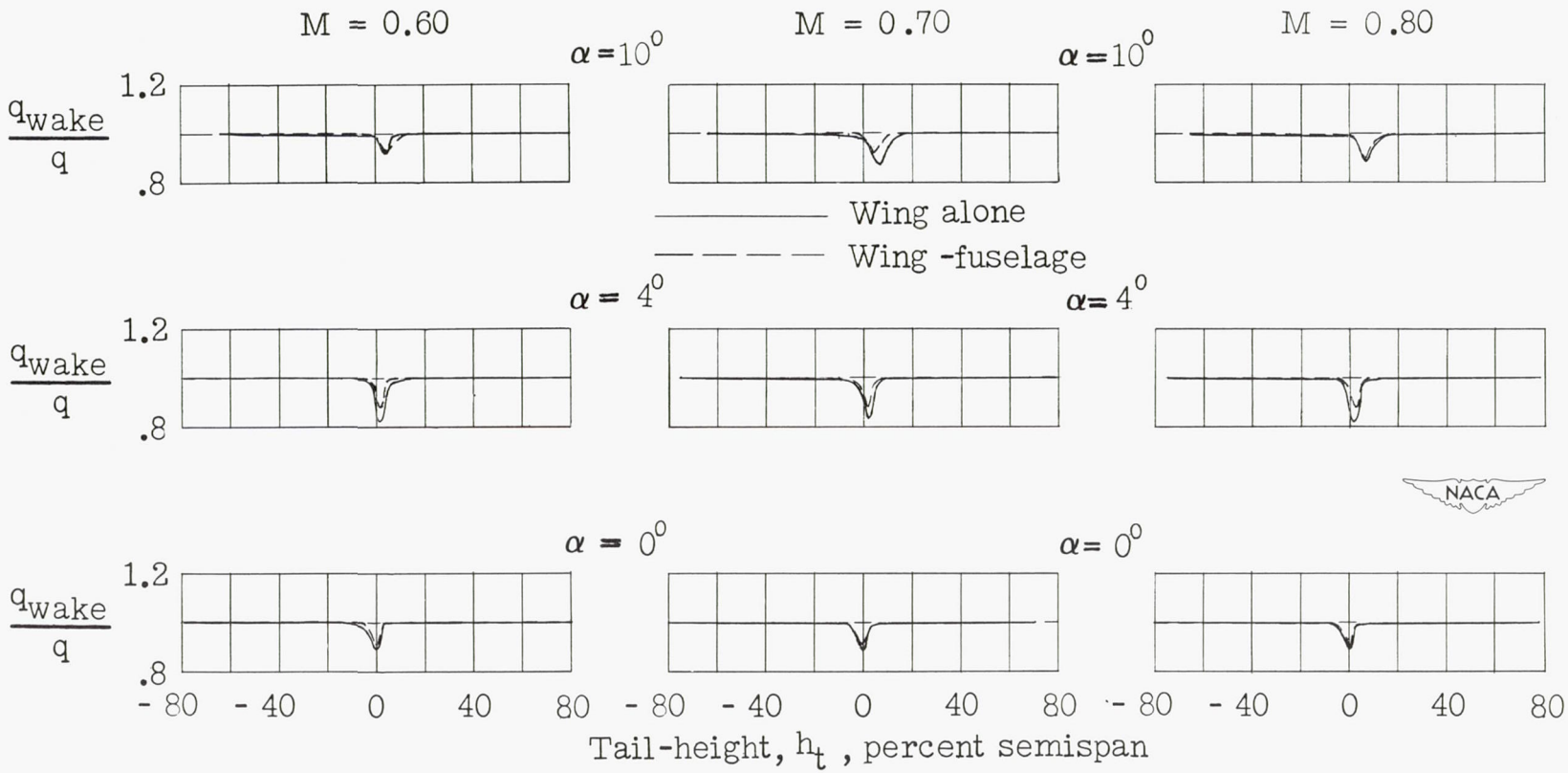

Figure 13.- Dynamic-pressure surveys in region of tail plane for a model with 60° sweptback wing, aspect ratio 2, taper ratio 0.6, and NACA 65A006 airfoil.

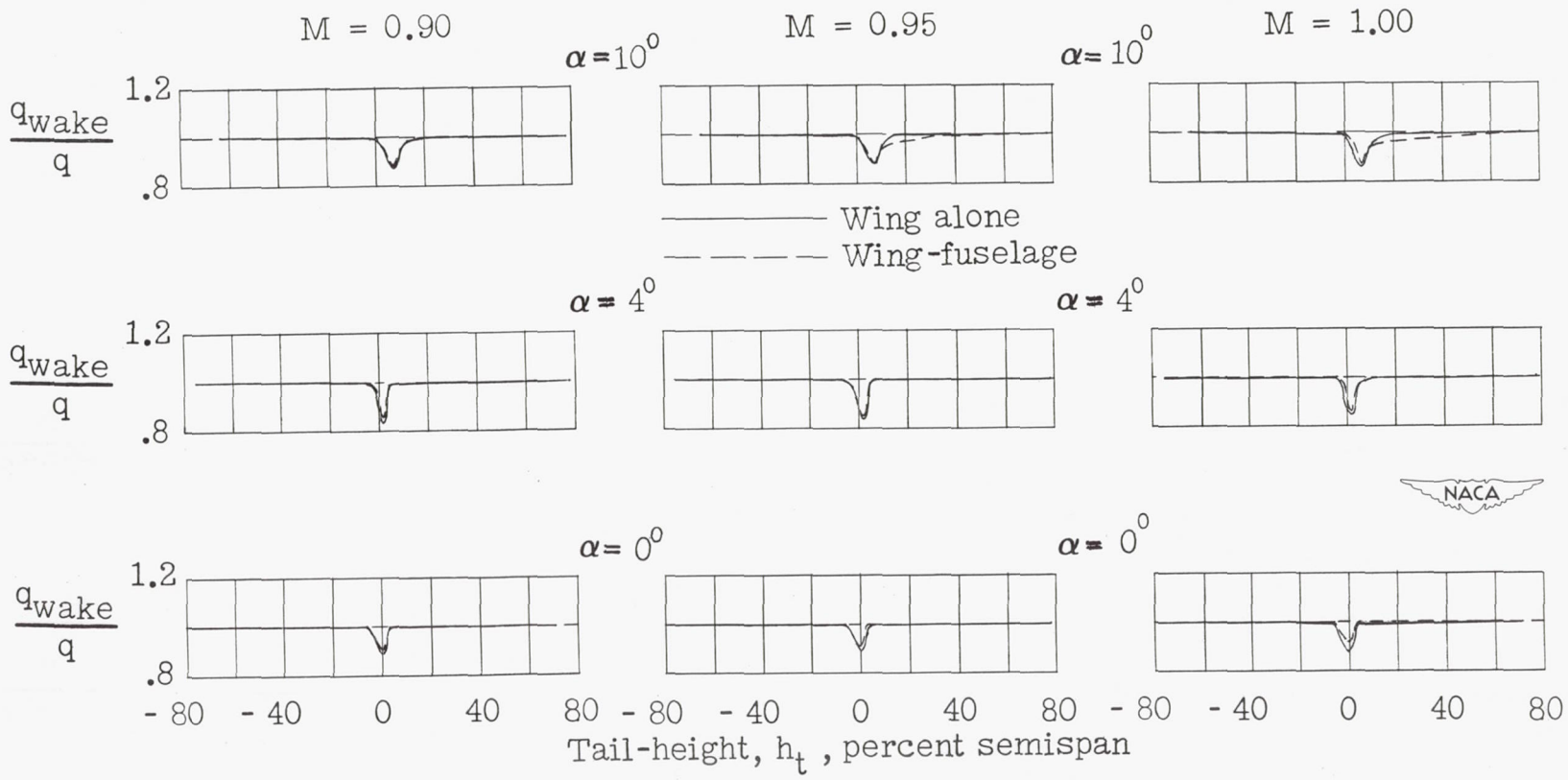

Figure 13.- Continued.

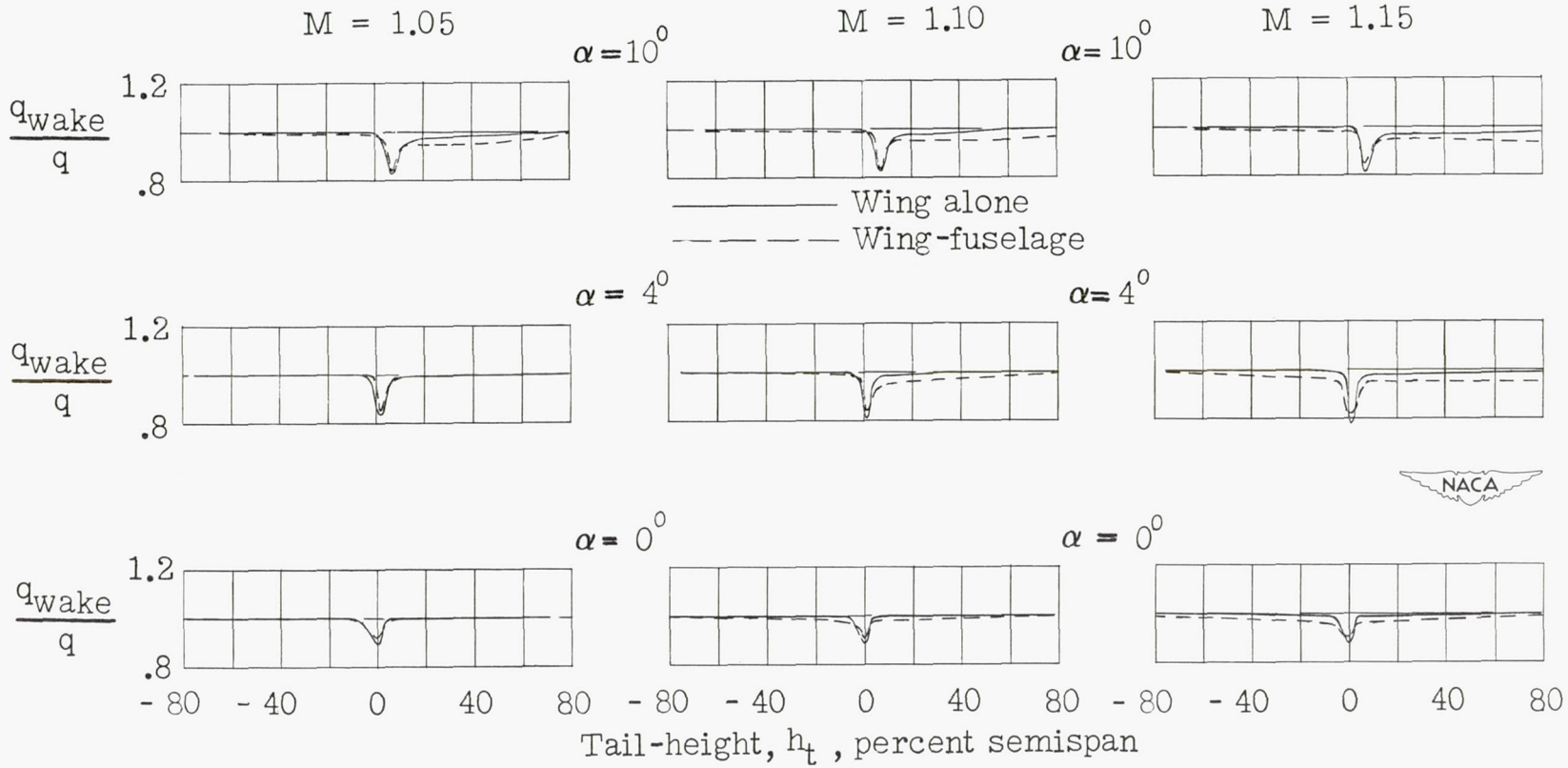

Figure 13.- Concluded.

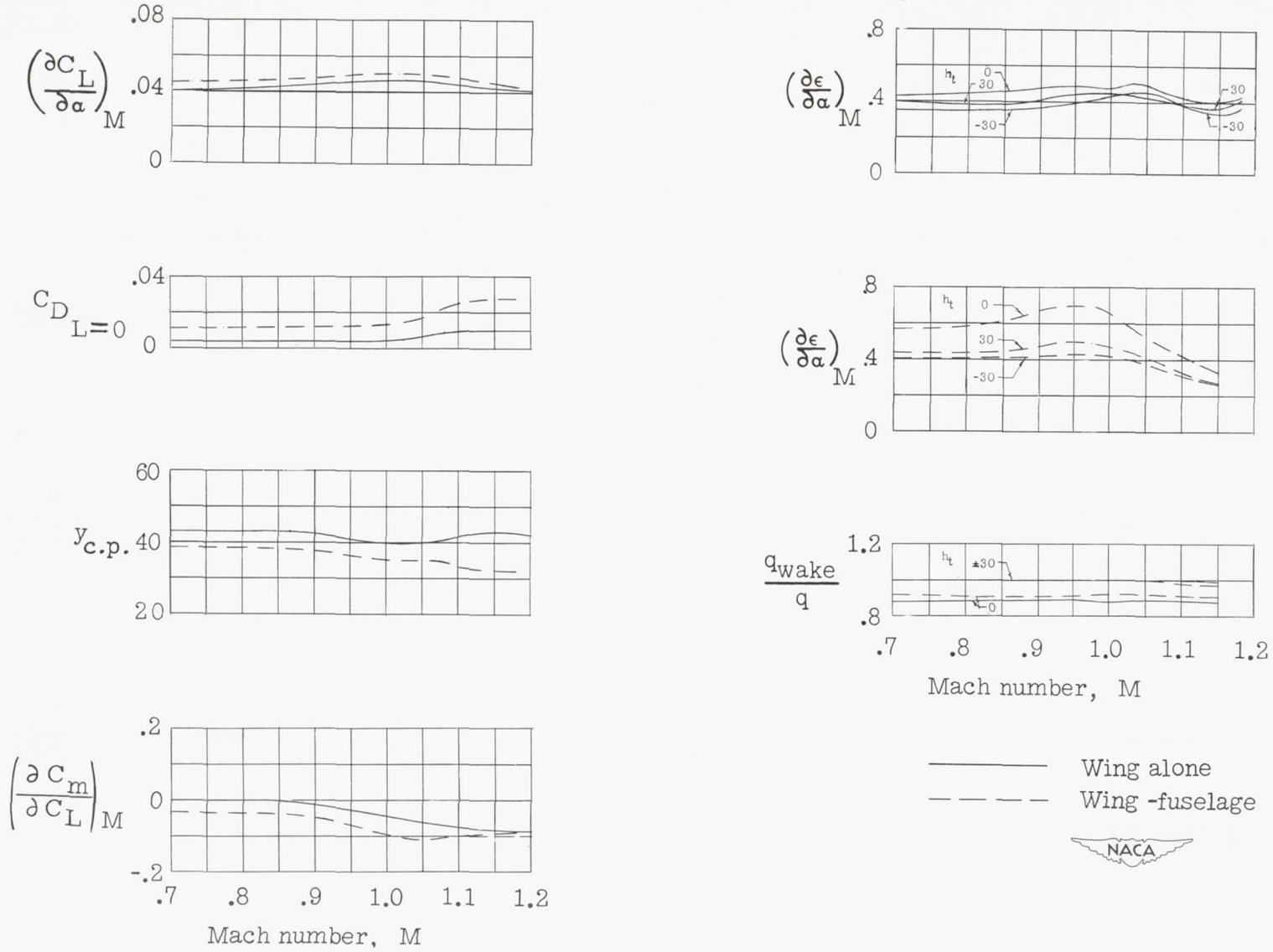

Figure 14.- Summary of aerodynamic characteristics for a model with 60° sweptback wing, aspect ratio 2, taper ratio 0.6, and NACA 65A006 airfoil. $C_L = 0$.